CARBON 71 (2014) 206–217

Available at www.sciencedirect.com

ScienceDirect

journal homepage: www.elsevier.com/locate/carbon

Polypropylene/carbon nanotube nano/microcellular structures with high dielectric permittivity, low dielectric loss, and low percolation threshold

A. Ameli [a], M. Nofar [a], C.B. Park [a,*], P. Pötschke [b], G. Rizvi [c]

[a] Microcellular Plastics Manufacturing Laboratory, Department of Mechanical and Industrial Engineering, University of Toronto, 5 King's College Road, Toronto M5S 3G8, Canada

[b] Leibniz Institute of Polymer Research Dresden (IPF), Hohe Straße 6, D-01069 Dresden, Germany

[c] Faculty of Engineering and Applied Science, University of Ontario Institute of Technology, Oshawa L1H 7K4, Canada

ARTICLE INFO

Article history:
Received 12 November 2013
Accepted 18 January 2014
Available online 27 January 2014

ABSTRACT

Nano/microcellular polypropylene/multiwalled carbon nanotube (MWCNT) composites exhibiting higher electrical conductivity, lower electrical percolation, higher dielectric permittivity, and lower dielectric loss are reported. Nanocomposite foams with relative densities (ρ_R) of 1.0–0.1, cell sizes of 70 nm–70 μm, and cell densities of 3×10^7–2×10^{14} cells cm^{-3} are achieved, providing a platform to assess the evolution of electrical properties with foaming degree. The electrical percolation threshold decreases more than fivefold, from 0.50 down to 0.09 vol.%, as the volume expansion increases through foaming. The electrical conductivity increases up to two orders of magnitude in the nanocellular nanocomposites ($1.0 > \rho_R > \sim 0.6$). In the proper microcellular range ($\rho_R \approx 0.45$), the introduction of cellular structure decreases the dielectric loss up to five orders of magnitude, while the decrease in dielectric permittivity is only 2–4 times. Thus, microcellular composites containing only ~0.34 vol.% MWCNT present a frequency-independent high dielectric permittivity (~30) and very low dielectric loss (~0.06). The improvements in such properties are correlated to the microstructural evolution caused by foaming action (biaxial stretching) and volume exclusion. High conductivity foams have applications in electromagnetic shielding and high dielectric foams can be developed for charge storage applications.

© 2014 Elsevier Ltd. All rights reserved.

1. Introduction

In the past decade, carbon nanotube (CNT) based nanocomposites have been of great interest in developing new generation of materials exhibiting unique combinations of properties and functionalities [1–6]. This has been realized due to the highly superior mechanical properties (strength of 100–300 GPa and elastic modulus of up to 1TPa) [7], and high electrical and thermal conductivity of CNTs [8,9]. One major class of such nanocomposites is being developed based on the electron transport phenomena of CNTs. Efforts are being devoted to achieve high electrical conductivity at low CNT loadings [10–13], which can be used in a variety of applications such as electromagnetic interference (EMI) shielding [14–19]. Compared to the composites of micro-sized additives (e.g., carbon fiber and carbon black), such nanocomposites present much lower electrical percolation thresholds [10–13] and superior EMI shielding effectiveness [14–19].

* *Corresponding author:* Fax: +1 416 978 0947.
E-mail address: park@mie.utoronto.ca (C.B. Park).

http://dx.doi.org/10.1016/j.carbon.2014.01.031
0008-6223/© 2014 Elsevier Ltd. All rights reserved.

Charge storage is another application that has been recently paid considerable attention, and efforts have been focused to develop polymer-based dielectrics with high dielectric permittivity (ε') and low dielectric loss ($\tan\delta$) [20–24]. However, the dielectric permittivity of polymers is very low ($\varepsilon' < 5$) [1,4] and achieving a high ε' and low $\tan\delta$ in a polymer system remains challenging. One approach is to add ceramic fillers, which can increase ε' of polymer by about ten times at loadings close to 50 vol.% [25–27]. However, ceramic fillers at such loadings are detrimental to the composites' mechanical performance. In percolative polymer nanocomposites (e.g., polymer-CNT), even though ε' significantly increases near the percolation threshold, this increase is usually accompanied with a huge increase in $\tan\delta$, due to the insulation-conduction transition, which restricts their further application toward dielectrics. Some people have tried to develop strategies to resolve this issue [20,21,24]. Yang et al. coated multiwalled CNTs (MWCNTs) with polypyrrole by an inverse micro-emulsion polymerization to screen charge movement and shut off leakage current [20]. They reported ε' of 44 and $\tan\delta$ of 0.07 for 10 wt.% MWCNT loading [20]. Liu et al. also used surface modification of MWCNTs followed by sonication and electrospinning with a rotating collector to prepare arrayed MWCNT-polysulfone dielectric nanocomposites [21]. They reported similar dielectric properties as those of [20] when 20 vol.% MWCNT is used [21]. They related the changes in ε' and $\tan\delta$ to the orientation and dispersion of MWCNTs. However, the required MWCNT loading still remains rather high (10 wt.% [20] and ~20 vol.% [21]).

Recently, foaming has shown promises in promoting the conductive nanocomposites for various applications. The introduction of foaming not only reduces the matrix weight significantly, but also can positively affect the electrical properties. In foaming with physical blowing agent such as supercritical carbon dioxide ($scCO_2$), the dissolved gas improves the dispersion [28] and distribution [29–31] of the fillers during processing. Some works have investigated the electrical properties of foamed composites [32–35], especially for EMI shielding applications [16,36–38]. Xu et al. developed conductive polyurethane/CNT (2 wt.%) composite foams with relative densities of less than 0.1 [33]. Recently, Tran et al. have investigated the relationships between the foams morphology and their electrical conductivity in poly(methyl methacrylate) (PMMA)/MWCNT composites and showed that the conductivity increases with expansion ratio [35]. Yang et al. have also reported the development of polystyrene/CNT (7 wt.%) composite foams with a fixed density of 560 kg m^{-3} for EMI shielding applications [16]. Thomassin et al. have developed polycaprolactone/MWCNT nanocomposites with loading as low as 0.25 vol.% for efficient EMI reduction [36,37].

Further to the density reduction, some works have demonstrated that foaming can decrease the electrical percolation threshold of conductive polymer composites [31,39–41]. Hermant et al. showed that a low percolation threshold is achieved in the foamed polymer composites of CNT prepared by polymerized high internal phase emulsions [39]. Zhang et al. also reported a slight decrease in the percolation threshold, when PMMA/graphene composite was foamed [40]. Recently, Ameli et al. [30,31] showed that the physical foaming in injection molding process decreases the percolation threshold and enhances the electrical conductivity and EMI shielding effectiveness of polypropylene (PP)/carbon fiber composites. However, the electrical conductivity of MWCNT nanocomposite foams has not yet been systematically investigated in a wide range of foaming degree, and to the best knowledge of the authors, no effort has yet been reported on the dielectric properties improvement of such foamed nanocomposites.

In this work, we report the preparation of micro/nanocellular PP/MWCNT nanocomposites with a wide range of relative density and cellular structure and characterize their electrical conductivity, dielectric permittivity, dielectric loss, microstructure, and cellular morphology. Here, we systematically demonstrate the reduction of electrical percolation threshold with the degree of foaming, and for the first time, we report that the PP-MWCNT nanocomposites with cellular structure exhibit remarkably lower dielectric loss as opposed to their solid counterparts. Furthermore, the relationships between the electrical/dielectric properties and microstructure are investigated.

2. Experimental

Commercially available injection grade homopolymer PP, Moplen HP 400R (Lyondell Basell Industries), having a melt flow rate of 25 dg min^{-1} and a density of 0.9 g cm^{-3} was selected as the base resin. The PP was filled with MWCNTs of the type Nanocyl™ NC 7000 (Nanocyl S.A., Sambreville, Belgium), having a density of 1.75 g cm^{-3}, a carbon purity of 90%, a mean diameter of 9.5 nm and a mean length of 1.5 μm.

The composites were produced by melt mixing using a masterbatch (MB) step with 10 wt.% MWCNT on a Berstorff ZE25 twin-screw extruder with a screw length of 48D. The temperature profile was set to 180–200 °C and a rotation speed of 500 rpm and a throughput of 5 kg/h were used. Composites with 1.28 vol.% (2.5 wt.%) and 2.56 vol.% (5.0 wt.%) MWCNTs were produced in a second extrusion step by diluting the MB using the same processing conditions and a higher throughput of 10 kg/h. Composites containing lower contents were prepared from PP-1.28 vol.% MWCNT using a DSM twin screw compounder (15 ml) at 180–200 °C. The composites were then compression-molded into rectangular samples (60 × 13 × 2.1 mm) at a temperature and a pressing force of 210 °C and 5 kN, respectively and cut to 13 × 13 × 2.1 mm to measure the through-plane electrical resistivity.

A batch process with $scCO_2$ was used for foaming. The samples of 10 × 10 × 2.1 mm were first placed in a high-temperature pressure vessel using specially designed sample holders. CO_2 was then fed into the pressure vessel using a Teledyne ISCO high pressure syringe pump and the samples were saturated at a desired pressure and temperature for certain time intervals. Foaming was then induced by a rapid depressurization. In order to achieve a wide range of foam density and structure, the saturation pressure (15–30 MPa), temperature (140–155 °C) and time (10–80 min.) were varied. In the case of high expansions, the foamed samples were cut to 13 × 13 mm for the electrical conductivity measurements.

The amount of remaining agglomerates in the micrometer scale was visualized using thin sections of extruded strands

in transmission mode with an Olympus BH2 microscope. A transmission electron microscope (TEM), Hitachi H-7000, was also used to assess the MWCNT dispersion and orientation in the solid and foamed samples.

The foam density (ρ_f) was measured using the water-displacement method (ASTM D792-00) and relative density (ρ_R) was obtained with respect to the density of the solid nanocomposite precursor (ρ_s). To measure the cell size and cell density, the samples were cryo-fractured and the microstructures were examined using either a JEOL JSM-6060 or Hitachi S-5200 scanning electron microscope (SEM). The cell density was calculated from the SEM micrographs using *Cell density* = $(nM^2/A)^{3/2} \times (\rho_s/\rho_f)$, where n is the number of voids in the micrograph, and A and M are the area and magnification factor of the micrograph, respectively.

An Alpha-A high performance conductivity analyzer by Novocontrol Technologies GmbH & Co. KG was used to measure the through-plane electrical conductivity, dielectric permittivity, and dielectric loss of the solid and foamed composites at a voltage of 1 V and a frequency range of 10^{-1}–10^{+5} Hz. The device measures the specific resistivity based on the sample resistance and geometry and calculates the conductivity. At least four replications were carried out at each case and the average values are reported.

3. Results and discussion

3.1. Microstructure

Thin sections of extruded strands were visualized using optical microscopy to assess the amount of remaining agglomerates in the micrometer scale. Fig.1a–b depicts the transmission-mode micrographs of PP-1.28 vol.% MWCNT and PP-2.56 vol.% MWCNT nanocomposites, respectively. It is seen that a relatively uniform dispersion of MWCNTs was achieved and only some very small remaining agglomerates could be observed. The dispersion of MWCNTs in the nanometer scale was also evaluated using transmission electron microscopy (TEM). Fig. 1c shows the network of individual MWCNTs, dispersed in the PP matrix. A relatively uniform dispersion of individual nanotubes as well as some bundles is seen.

Fig. 2 depicts the cellular morphology of various PP-1.28 vol.% MWCNT nanocomposite foams and Fig. 3 shows their relative density, cell density, and average cell size. Relative density is a measure of foaming degree, defined as the ratio of foam density and its solid precursor density. Similar foaming results were obtained for the nanocomposites containing other MWCNT contents. By carefully controlling and tuning the foaming parameters (i.e., saturation temperature, pressure, and time), we were able to consistently decrease the relative density from 1 to 0.1 (Fig. 3a). This range of relative density resulted in the foams with a wide variety of cellular morphology, including conventional (i.e., cell sizes greater than 30 μm), microcellular (i.e., cell sizes between 30 and 1 μm) and nanocellular (i.e., cell sizes less than 1 μm and cell densities greater than 10^{13} cells cm^{-3}) foams. As seen in Fig. 3, the average cell size and cell density ranged from ~70 nm – 100 μm and 10^7–10^{14} cells cm^{-3}, respectively.

The nano/microcellular foams were obtained by saturating the samples at a pressure of 30 MPa and temperatures close to the melting temperature of the polypropylene. Table 1 summarizes the saturation temperature and time used in the foaming of the nano/microcellular PP-1.28 vol.% MWCNT nanocomposites of Fig. 2. At a certain pressure, by slightly decreasing the temperature or increasing the saturation time, the foam expansion decreased and samples with smaller cell sizes and larger cell densities were achieved. By further decrease of the saturation temperature below a critical temperature, the foam morphology shifted to the nanocellular regime and the foam expansion was further decreased. It is believed that these changes in the cellular morphology with the foaming temperature stemmed from the variations in the crystal structure of the polypropylene matrix that had been treated under different saturation temperatures. Fundamental investigations of the nanocellular foaming mechanisms are the subject of a future study. This wide range of the foaming properties provided a complete platform to investigate the effects of foaming degree on the electrical properties of the nanocomposites at different size scales.

3.2. Electrical conductivity and percolation

Foaming affected the electrical conductivity through two different mechanisms: (a) foaming action, i.e., the cell growth effect on the alignment and interconnection of the surrounding MWCNTs and (b) volume expansion, i.e., the effect of the localization of MWCNTs within the cell walls and struts due to the volume exclusion by cells. In order to differentiate the effects of these two mechanisms, the percolation analysis was conducted in two different ways. First, the volume expansion by foaming was excluded and the MWCNT volume percent was considered with respect to the volume of the polymer component only. In other words, the MWCNT

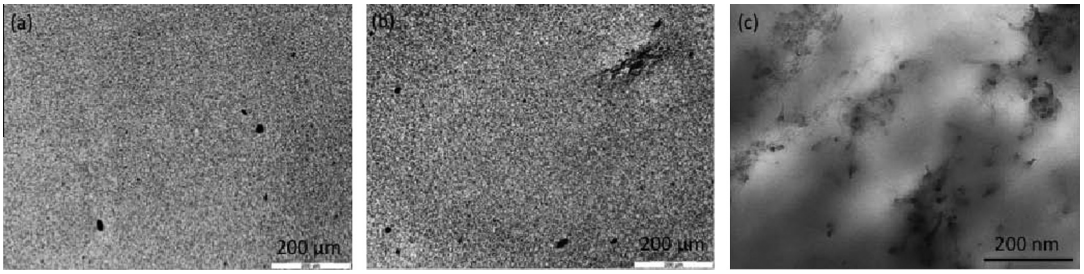

Fig. 1 – Transmission light microscopy on thin sections (5 μm) of extruded PP nanocomposites with (a) 1.28 vol.% and (b) 2.56 vol.% MWCNTs, and (c) TEM micrograph of PP-2.56 vol.% MWCNT. (A colour version of this figure can be viewd online.)

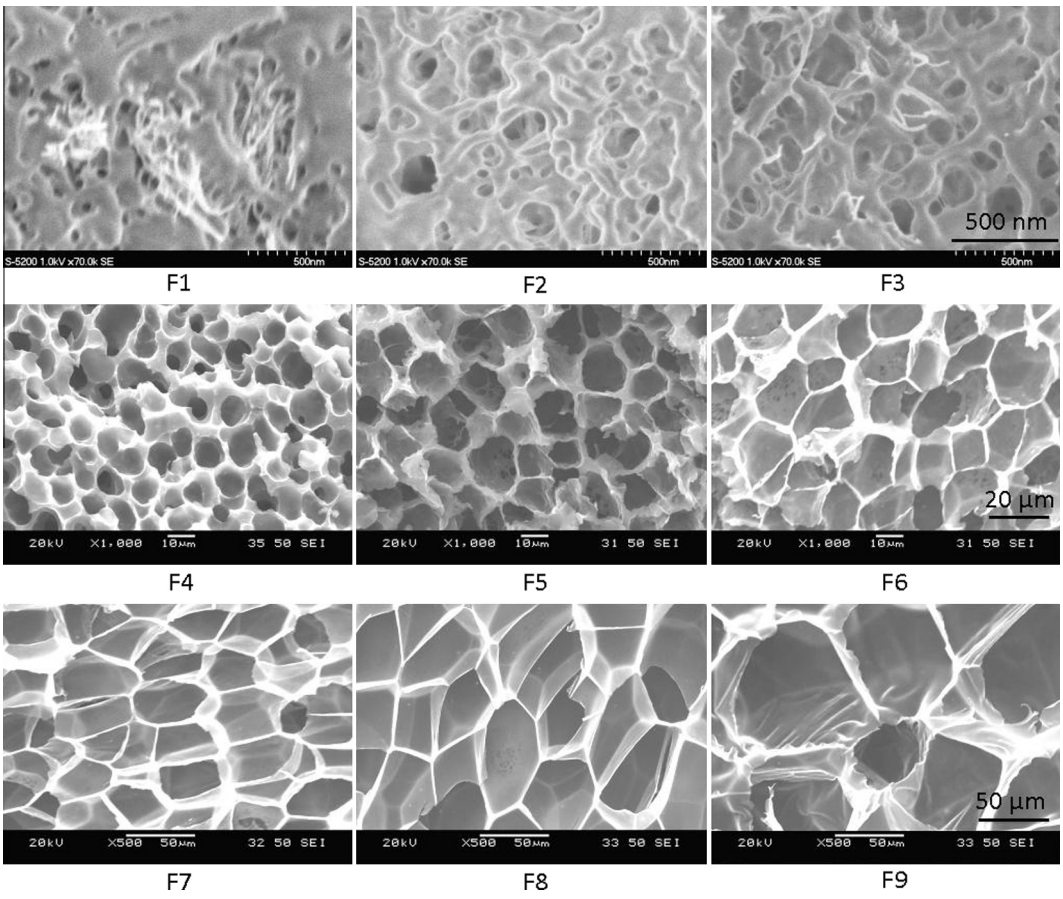

Fig. 2 – SEM micrographs of various nano/microcellular PP-1.28 vol.% MWCNT nanocomposites. Each row has the same magnification. (A colour version of this figure can be viewd online.)

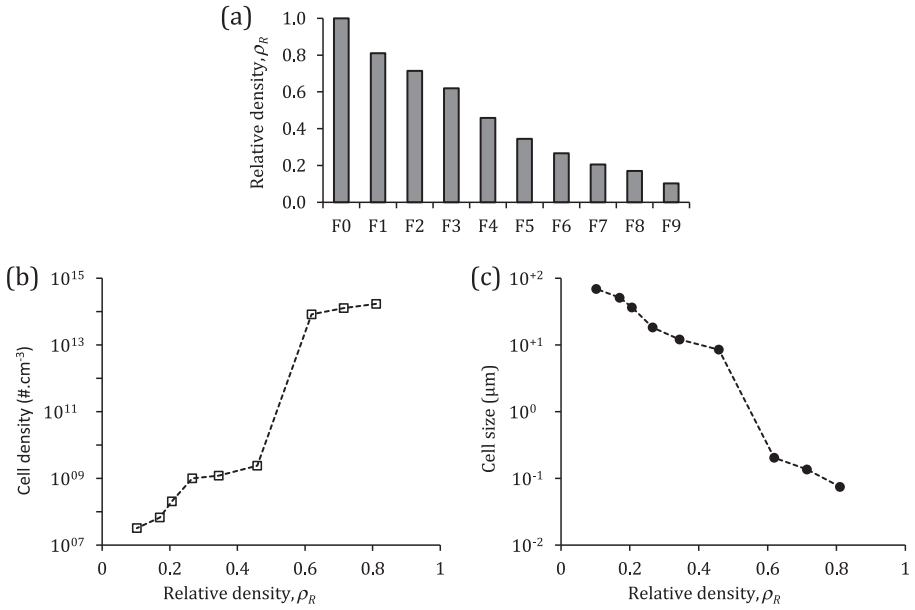

Fig. 3 – Relative density (a), cell population density (b), and average cell size (c) of the nano/microcellular PP-1.28 vol.% MWCNT nanocomposites of Fig. 2. (A colour version of this figure can be viewd online.)

Table 1 – Saturation temperature and time used in the foaming of the nano/microcellular PP-1.28 vol.% MWCNT nanocomposites of Fig. 2.

Foam	F1	F2	F3	F4	F5	F6	F7	F8	F9
Temperature	142	143	144	149	149	149	151	152	154
Time (min)	15	15	15	30	15	10	15	15	15

Table 2 – Maximum electrical conductivity (σ_{max}) and the corresponding optimum relative density of the nanocomposite foams ($(\rho_R)_{opt}$) at various MWCNT contents.

MWCNT content (vol.%)	Solid	Foam		
	σsolid	σmax	$(\rho_R)_{opt}$	σmax/σsolid
2.56	2.02×10^{-03}	1.29×10^{-02}	0.55	6.4
1.28	2.20×10^{-04}	1.70×10^{-03}	0.61	7.7
0.77	9.63×10^{-06}	1.27×10^{-04}	0.68	13.2
0.51	2.30×10^{-08}	7.15×10^{-06}	0.81	310.9

Table 3 – Percolation model parameters for solid and foamed nanocomposites of various relative densities. Initial and final threshold values are given based on the initial content and final content of MWCNT, respectively. R^2 is the coefficient of determination for the linear regression analysis of $\sigma = \sigma_0 (\varphi-\varphi_c)^t$ in the double-logarithmic scale.

ρ_R (–)	φ_c^i (vol. %)[a]	φ_c^f (vol. %)[b]	t	R^2
1.0	0.50	0.50	2.18	0.99
0.7	0.43	0.30	2.32	0.98
0.45	0.48	0.22	2.47	0.96
0.3	0.51	0.15	2.56	0.98
0.2	0.72	0.14	2.72	0.97
0.1	0.98	0.09	2.81	0.99

[a] φ_c^i was calculated with respect to the polymer volume only.
[b] φ_c^f was calculated with respect to the total foam volume.

volume percent of the foamed nanocomposites was taken the same as of their solid precursors. This volume percent was called "initial content". The percolation threshold values based on the initial content of MWCNT was termed "initial percolation threshold" (φ_c^i in Table 3). Percolation analysis with respect to the initial content determined the effect of foaming action only.

In order to assess the localization effect by volume expansion, the percolation curves were also analyzed against the "final content" of MWCNT. The final content was calculated as the MWCNT volume percent with respect to the total volume of the foamed sample (i.e., including both polymer and gas components). The percolation threshold values based on the final content of MWCNT was termed "final percolation threshold" (φ_c^f in Table 3).

3.2.1. *Effect of foaming action*

Fig. 4 depicts the variation of the electrical conductivity of the nanocomposite foams containing various MWCNT contents with relative density. Two regions could be clearly identified in the relationship between the electrical conductivity and the relative density. First, the electrical conductivity increased with the decrease of the relative density up to an optimum

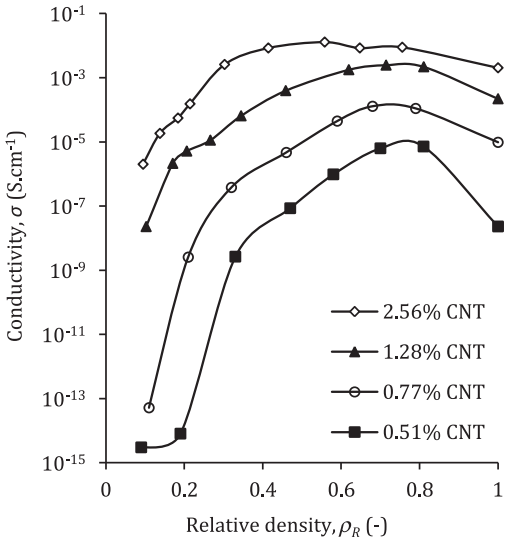

Fig. 4 – Electrical conductivity of nano/microcellular PP nanocomposites with different vol.% MWCNT as a function of relative density. (A colour version of this figure can be viewd online.)

relative density, which resulted in the maximum conductivity value, up to two orders of magnitude higher than that of the corresponding solid sample. Then, the electrical conductivity started to decrease by further decrease of the relative density. It is also noted that the optimum relative density decreased as the MWCNT content increased (Table 2). In other words, the nanocomposites containing higher filler content could be expanded more prior to reaching the maximum electrical conductivity. On the other hand, the conductivity raise was greater at the lower MWCNT contents with lower conductivity values (Table 2). At the optimum relative density, the conductivity of PP-2.56 vol.% MWCNT increased by 6.4 times while that of PP-0.51 vol.% MWCNT increased by more than 300 times, compared to those of the solid precursors.

Fig. 5 shows the electrical conductivity with respect to the initial content of MWCNT at several relative densities. According to the percolation theory, the power law equation $\sigma = \sigma_0\ (\varphi - \varphi_c)^t$ can be applied for $\varphi > \varphi_c$ where σ and σ_0 are the measured conductivity and a scaling factor, respectively, φ is the filler volume content, φ_c is the filler electrical percolation threshold, and t is a critical exponent related to the filler distribution, dispersion and dimensionality. The value of φ_c was obtained by finding the best linear fit of the theory to the experimental data in the double-logarithmic scale. The electrical percolation threshold for the solid samples was found to be 0.50 vol.% at which the insulation-conduction transition occurred and the conductivity increased by several orders of magnitude. This value is in the range reported for polymer composites containing MWCNTs [42,43]. In the case of low void fraction foams ($\rho_R = 0.70$), the electrical conductivity of all nanocomposites containing various MWCNT contents increased after the introduction of foaming (Fig. 5). According to the percolation analysis, this increase in the electrical conductivity resulted in a decrease of the percolation threshold from 0.50 to 0.43 vol.% (φ_c^i in Table 3). However,

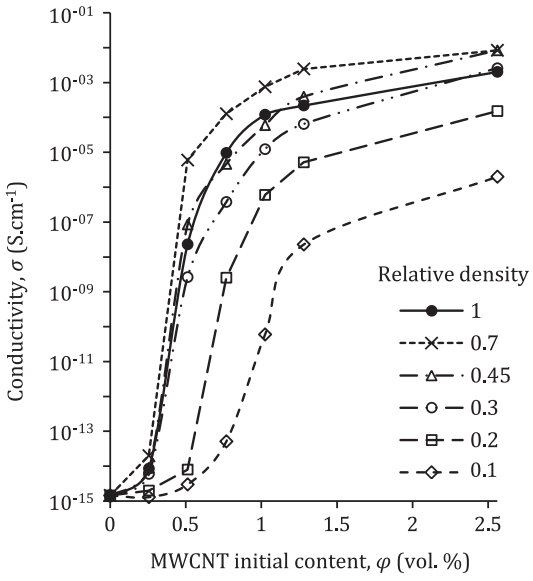

Fig. 5 – Variations of the electrical conductivity with MWCNT initial content at several relative densities. Some of the data points were extracted from Fig. 4. (A colour version of this figure can be viewd online.)

as the relative density was decreased from 0.7 to 0.1, the percolation threshold was consistently increased from 0.43 to ~1.0 vol.%.

In the solid nanocomposites, the MWCNTs were randomly distributed and oriented and thus their alignment was considered isotropic (Fig. 6I(a)). By the introduction of foaming, the nanotubes around each growing cell started to displace and rotate. The degree of nanotube displacement/rotation depended on its initial relative location/alignment with respect to the cell nucleus. The spherical growth of cell exerted biaxial stretching on the polymer matrix surrounding the cell and thus disturbed the isotropic alignment of the MWCNTs. This biaxial stretching was proportional to the degree of foaming. As the degree of foaming increased, the biaxial stretching applied to the polymer matrix also increased, which led to the more significant alignment of MWCNTs around the cells. In foams with higher relative densities, the lower degree of foaming caused only slight alignment of MWCNTs around the cells as shown in Fig. 6I(b). In the case of foams with lower ρ_R, however, the MWCNTs were fully oriented normal to the cell radius due to the excessive biaxial stretching (Fig. 6I(c)). In other words, in this case, the alignment reduced from 3-D to 2-D state [6,28]. Such sever alignment of nano-additives around the cells has already been clearly demonstrated for nanoclay [28].

Fig. 6II schematically illustrates the evolution of the MWCNT interconnections with foaming. During foaming, the biaxial stretching caused the MWCNTs to slightly orient around the cells while the cell-to-cell compression forced them to decrease their distance. This action increased the MWCNT interconnections (Fig. 6II(b)) and thereby increased the electrical conductivity (Fig. 4, higher ρ_R range). However, as the degree of foaming was further increased beyond an optimum point, the MWCNTs became fully oriented normal to the cell radius (similar to planar orientation) (Fig. 6II(c)) and excessive stretching resulted in their dilution and thus the loss of the interconnections. Consequently, the conductivity started to decrease (Fig. 4, lower ρ_R range). Beyond this point, the conductivity proportionally decreased with ρ_R, which can be explained by further loss of the MWCNT interconnections. Similar trend of conductivity with filler alignment has been previously reported for solid nanocomposites. It has been demonstrated that neither a fully isotropic distribution nor a complete alignment is the best state of orientation to achieve the highest conductivity [44–46]. Du et al. have shown that the maximum conductivity is achieved when some degree of alignment is introduced to PMMA-single walled CNT (SWCNT) nanocomposites [44]. They also reported that this degree of alignment increases as the CNT content increases, similar to the findings reported in Fig. 4. Our work is also consistent with the analytical results of Munson-McGee showing the probability of one cylinder intersecting any number of others in an ensemble of cylinders [45]. Another factor that might have contributed to the increase of electrical conductivity is a better dispersion of the MWCNT when nanocomposite was foamed using a physical blowing agent [28].

3.2.2. *Effect of volume expansion*

Fig. 7 shows the conductivity of the foamed nanocomposites with respect to the final MWCNT content. Table 3 also lists

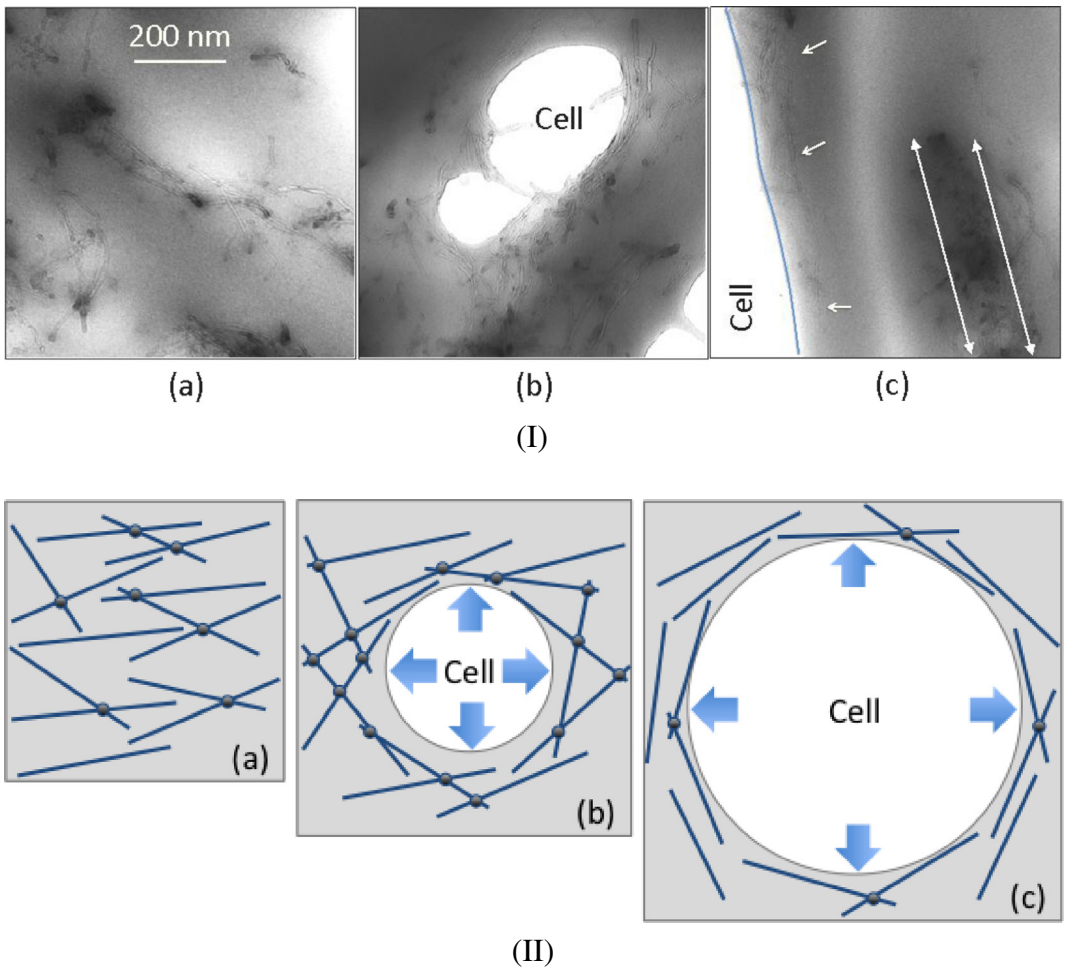

Fig. 6 – (I) TEM images illustrating MWCNT alignment in solid (a), low expansion foam (ρ_R = 0.7) (b), and high expansion foam (ρ_R = 0.2) (c) of PP-1.28 vol.% CNT nanocomposites. (II) 2-D conceptualization of the evolution of MWCNT interconnection with foaming: solid (a), low expansion (ρ_R = 0.7) (b), and high expansion (ρ_R = 0.2) (c). (A colour version of this figure can be viewd online.)

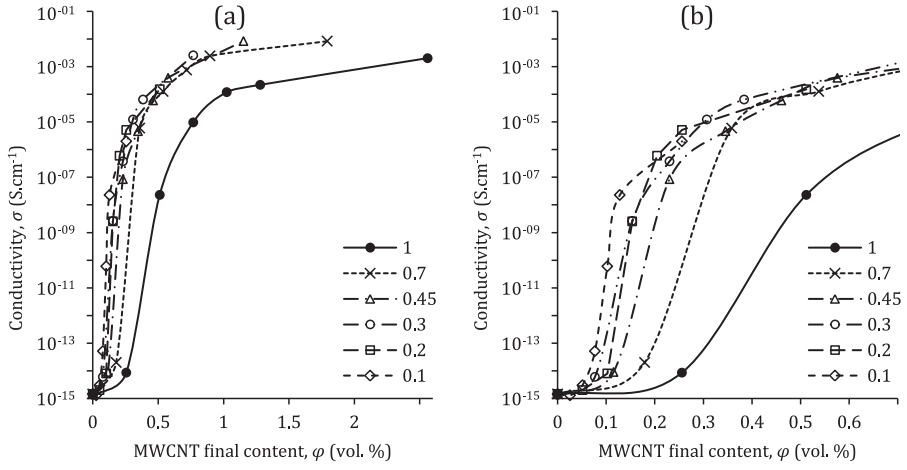

Fig. 7 – Variations of the electrical conductivity with MWCNT final content of (a) 0–2.5 vol.% and (b) 0–0.7 vol.%, at several relative densities. (A colour version of this figure can be viewd online.)

the initial and final percolation threshold values with respect to the polymer volume and final foam volume, respectively. The final percolation threshold was consistently decreased as the relative density was decreased. The lowest percolation threshold was measured to be 0.09 vol.% at the highest expansion ($\rho_R = 0.1$), which was five times lower than φ_c of the solid samples (i.e., 0.50 vol.%). This significant decrease of the percolation threshold stemmed from the localization of the nanotubes in a partial volume of the sample (i.e., polymer component only, not gaseous part), as has been also discussed in [35].

Based on the coefficient of determination (R^2 value in Table 3), it is seen that all the solid and foamed nanocomposites followed the percolation power law with an acceptable accuracy. The percolation analysis resulted in a t value of about 2.18 for solid samples that is in a relatively good agreement with the theoretical value $t \cong 2$ for a three dimensional percolation network [47,48] and the experimental values reported in the literature for solid nanocomposites [49]. Furthermore, as the relative density decreased, t value increased and further deviated from its theoretical value. The theoretical value of t is obtained based on the assumption of a uniform and isotropic distribution of the conductive filler. Upon foaming, the fillers were localized and forced to take an ordered orientation around the cells, which was further pronounced at higher expansions. Therefore, the higher t values for the foamed samples might have been an indication of a different state of the filler distribution and alignment, which was more selective rather than being uniform and isotropic. Higher t values have also been reported for superstructures with a fractal characteristic or formation of a secondary network [50,51].

It is noted that the foams at only ~0.1 vol.% MWCNTs (Fig. 7) satisfies the conductivity range required for electrostatic dissipation and electromagnetic painting applications [40,52]. Also, at MWCNT contents greater than 0.4 vol.%, the conductivity increases to a range (10^{-3}–10^{-2} S cm^{-1}) that may be sufficient for EMI shielding applications where a low shielding effectiveness (15–20 dB) is required [31,36,40]. Furthermore, in low expansion range, while the filler content was decreased, the conductivity value could also be increased, which is again favorable for EMI applications.

3.3. *Dielectric permittivity and loss*

Fig. 8 depicts the variations of the dielectric permittivity (ε') and dielectric loss ($\tan\delta$) in the solid and foamed ($\rho_R = 0.45$) nanocomposites at various MWCNT contents. MWCNT contents reported in this section are "initial contents", unless otherwise stated. At lower filler contents, the addition of MWCNT did not change the stability of the dielectric permittivity, as seen on a frequency-independent behavior. As the

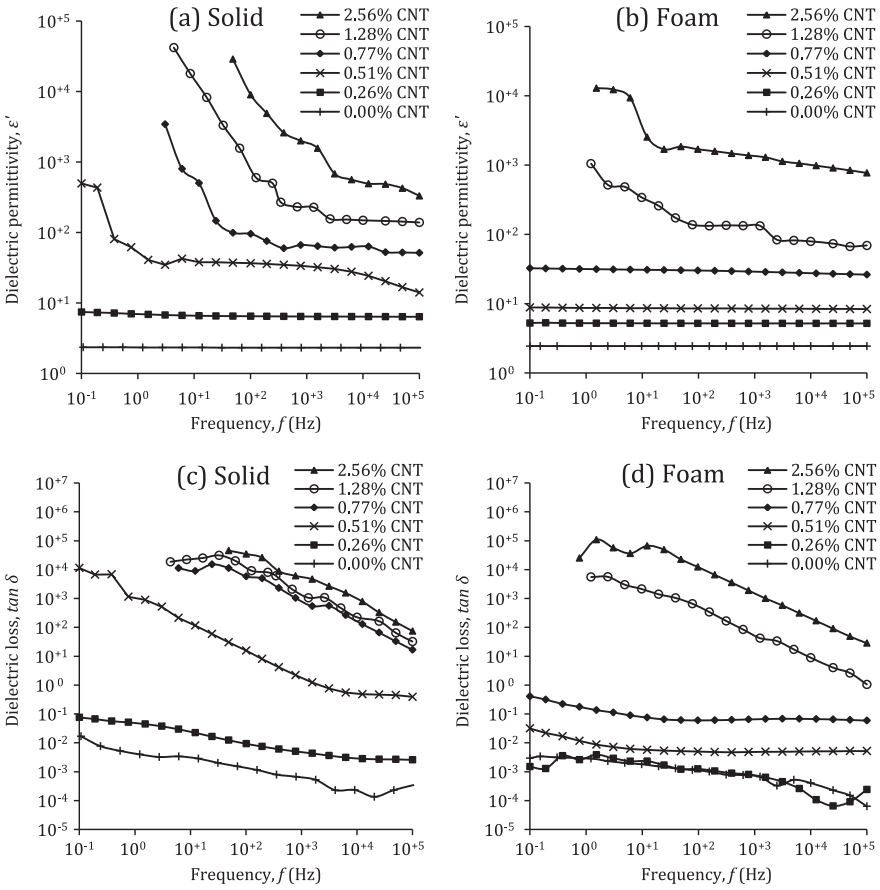

Fig. 8 – Broadband dielectric permittivity of solid (a) and foamed (b) PP-MWCNTs nanocomposites and dielectric loss of solid (c) and foamed (d) PP-MWCNTs. (A colour version of this figure can be viewd online.)

MWCNT content was increased, the permittivity started to exhibit a frequency-dependent behavior. In this regime, the permittivity initially decreased by several orders of magnitude with the increase of frequency until it reached a crossover frequency beyond which remained approximately unchanged. As seen in Fig. 8a–b, this crossover frequency had larger values for the composites having a higher MWCNT content. Similar trends have been reported for other conductive composites [31,49,53]. The dielectric loss also showed relatively similar characteristics as that of the dielectric permittivity. In the solid samples, the dielectric loss was relatively frequency-independent at lower MWCNT contents. However, it became highly sensitive to frequency as the filler content approached the electrical percolation threshold [20].

Fig. 9a–b gives the dielectric permittivity and loss for the solid and foamed nanocomposites, measured at 100 Hz, as a function of MWCNT content. In the solid nanocomposites, the dielectric permittivity continuously increased from 2.4×10^0 to 3.0×10^3 with the increase of MWCNT content, which is consistent with [20,49]. As foaming with $\rho_R = 0.45$ was introduced to the samples, their dielectric permittivity was decreased by 2–4 times (Fig. 9a). For example, at 0.77 vol.% MWCNT, the dielectric permittivity of the solid samples was decreased from 96 to 30 when foaming was applied. However, the high dielectric permittivity ($\varepsilon' = 96$) of the solid PP-0.77 vol.% MWCNT was frequency-dependent (Fig. 8a) while that of the foamed counterpart revealed a frequency independent behavior.

Another important requirement for the dielectrics is the low dielectric loss. As seen in Fig. 9b, the dialectic loss of the solid samples increased dramatically with the MWCNT content. Specifically, near the percolation threshold, when the MWCNT content was increased from 0.26 to 0.77 vol.%, the dielectric loss of the solid samples was hugely increased (up to 6 orders of magnitude) and possessed a decreasing trend with frequency (Fig. 8c). Unlike the high dielectric permittivity of the solid samples at high filler loadings, their very high dielectric loss limits their application as dielectric materials.

The dielectric loss of the samples, however, significantly decreased when the foaming was introduced (Fig. 9b). The dielectric loss of the foamed PP-0.26 vol.% MWCNT ($\tan\delta = 1.2 \times 10^{-3}$) was even lower than that of the neat PP ($\tan\delta = 1.8 \times 10^{-3}$), while its permittivity was more than twice as that of the neat PP. Near the percolation threshold, when the MWCNT content was increased from 0.26 to 0.77 vol.%, the dielectric loss of the foamed samples increased only slightly, i.e., from 1.2×10^{-3} to 6.1×10^{-2} and they had a frequency-independent behavior (Fig. 8d). At 0.77 vol.% MWCNT, the dielectric loss of the foamed nanocomposite was five orders of magnitude lower than that of the corresponding solid counterpart. It is noted that even though beyond 0.77 vol.% MWCNT, the dielectric loss of the foamed samples suddenly increased, it was still lower than their corresponding solid ones.

Since a high dielectric permittivity together with a low dielectric loss is the pursued combination for dielectrics, the ratio of $\varepsilon'/\tan\delta$ is an indication of the overall performance and high values indicate better performance. Fig. 9c compares this ratio for the solid and foamed composites. It is seen that below 1.28 vol.% MWCNT, the dielectric performance of the foamed samples was highly superior to those of the corresponding solid ones. The largest improvement in the dielectric performance through foaming was found for

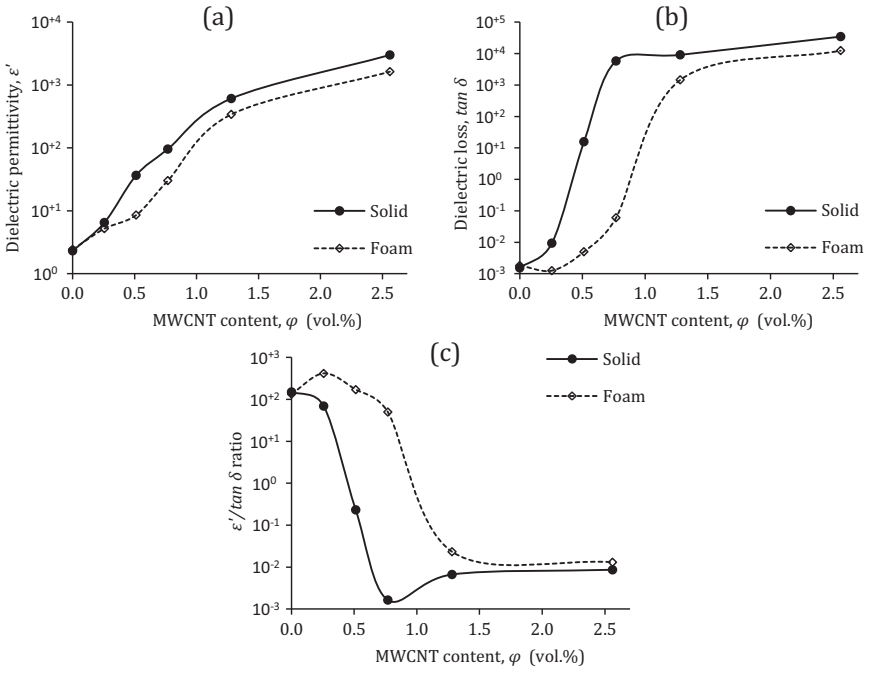

Fig. 9 – Dielectric permittivity (a), dielectric loss (b), and ratio of dielectric permittivity/loss (c) for solid and foamed PP-MWCNT nanocomposites, measured at a frequency of 100 Hz. (A colour version of this figure can be viewd online.)

PP-0.77 vol.% MWCNT, where the ratio of $\varepsilon'/\tan\delta$ increased from 1.65×10^{-2} to $5.02\times10^{+2}$, more than four orders of magnitude. This corresponded to the stable $\varepsilon' \approx 30$ and $\tan\delta \approx 0.06$ of the foamed sample as opposed to the frequency-dependent $\varepsilon' \approx 96$ and $\tan\delta \approx 5.8\times10^{+3}$ of solid samples. Considering the volume expansion effect ($\rho_R \approx 0.45$), the final filler content in our PP-0.77 vol.% MWCNT was about 0.34 vol.%. Recently, Yang et al. [20] and Liu et al. [21] reported $\varepsilon' = 44$ and $\tan\delta \approx 0.07$ for nanocomposites with a high content of 8 wt.% [20] and ~20 vol.% [21] MWCNT, and using specifically designed synthesis procedures. Here, we report similar results with using only 0.34 vol.% MWCNT for the nanocomposites made using melt compounding followed by physical foaming.

The dielectric permittivity is mainly affected by the polarization (localized charges) inside the material. In conductive composites, polarization of matrix, conductive filler and interfacial polarization all can play role depending on the frequency range [54–57]. The polymer matrix polarization however can be effective only at optical frequency range. Therefore, in the frequency range tested here, the variations of the permittivity should be originated from the polarization of the matrix/nanotube interface and/or polarization of the nanotubes [54–56]. The fact that the dielectric permittivity at low frequencies increased significantly only when the MWCNT content reached the percolation threshold indicates that the permittivity enhancement is largely due to the interfacial polarization. According to the Maxwell Wagner Sillars (MWS) effect [58,59], when a current flows across the two-materials interfaces, charges can be accumulated at their interface and the giant increase in the permittivity caused by this effect is expected to occur near the percolation threshold [31,54]. In the nanocomposites, the nanotubes were separated by thin barriers of dielectric regions (i.e., PP matrix), and the adjacent nanotubes formed a nano-capacitor. As the filler content was increased near the percolation threshold, the dielectric barrier thickness was decreased and the effective surface increased drastically [31,54,58]. However, in the solid nanocomposites, as the MWCNT content increased, the interconnections between the nanotubes also increased, as indicated by the increased electrical conductivity (Fig. 5), and this, in turn, resulted in the significant current leakage and thus the dielectric loss was dramatically increased [20,49].

When the foaming with relatively low expansion ratio (~0.45 here) was introduced to the nanocomposites, it changed the microstructure favorably to having better dielectric properties. As explained in section 2.2.1, upon the cell growth, the nanotubes between the adjacent cells experienced biaxial stretching and uniaxial compression. The stretching action eventually forced the nanotubes to take an in-plane orientation normal to the cell radius, which decreased the nanotube's interconnections, if sufficient degree of cell growth is provided (Fig. 6I(c) and II(c)). At the same time, the compression action over the cell walls forced the aligned nanotubes to decrease their interspace distances. Furthermore, the volume exclusion by foam expansion increased the local concentration of nanotubes while foaming action assured that excessive interconnection between nanotubes was prevented. This action further decreased the nanotubes' interspace distances. The decreased nanotube's interconnections resulted in a slight decrease of permittivity but the new structural configuration was very effective in shutting off the current leakage and storing the charges, as also explained in [20,21], and thus the dielectric loss was dramatically decreased.

4. Summary

Nano/microcellular PP/MWCNT nanocomposites exhibiting higher electrical conductivity, lower electrical percolation, higher dielectric permittivity, and lower dielectric loss are reported. The PP/MWCNT nanocomposites were prepared by melt compounding and the cellular structure was introduced by foaming using $scCO_2$. In order to provide a complete platform to assess the evolution of electrical and dielectric properties with foaming, relative densities (ρ_R) of 1.0–0.1, cell sizes of 70 nm – 70 μm, and cell densities of 3×10^7 – 2×10^{14} cells cm^{-3} were successfully achieved. Electrical conductivity, dielectric permittivity, and dielectric loss of the samples were measured and the microstructure and cellular morphology of the solid and foamed composites were characterized using transmission and scanning electron microscopies, respectively.

A density-dependent electrical conductivity was observed for the foamed nanocomposites. The electrical conductivity first increased up to two orders of magnitude as the relative density was decreased (nanocellular range, $1.0 > \rho_R > \sim0.6$). Upon further decrease of the relative density, the electrical conductivity started to decrease (microcellular range, $\sim0.6 > \rho_R > 0.1$). These changes were explained in terms of the effect of foaming action (biaxial stretching) on the alignment and interconnection of MWCNTs. Through the volume exclusion caused by foaming, the final percolation threshold of PP/MWCNT nanocomposites was decreased from 0.50 to 0.09 vol.%, more than five times.

In a proper foaming range ($\rho_R \approx 0.45$), the introduction of microcellular structure decreases the dielectric loss up to five orders of magnitude, while the decrease in dielectric permittivity is only 2–4 times. Unlike the solid nanocomposites, the microcellular foams exhibited a frequency-independent dielectric characteristic up to a permittivity of about 30. PP foams containing only ~0.34 vol.% MWCNT presented a high dielectric permittivity (~30) and very low dielectric loss (~0.06). The improvements in dielectric properties were attributed to the decreased interconnections and interspace distances between MWCNTs caused by biaxial stretching and uniaxial compression effects of foaming action.

The results of this work reveal that microcellular structures created through foaming can be effectively used to develop new materials for efficient EMI shielding as well as charge storage applications.

Acknowledgements

The work was financially supported by MITACS, Ontario and NSERC, Canada. We thank Mr. Kretzschmar (IPF) for the material extrusion.

REFERENCES

[1] Chu BJ, Zhou X, Ren KL, Neese B, Lin MR, Wang Q, et al. A dielectric polymer with high electric energy density and fast discharge speed. Science 2006;313(5785):334–6.

[2] Ozaki M, Shimoda Y, Kasano M, Yoshino K. Electric field tuning of the stop band in a liquid-crystal-infiltrated polymer inverse opal. Adv Mater 2002;14(7):514–8.

[3] Harkema S, Steiner U. Hierarchical pattern formation in thin polymer films using an electric field and vapor sorption. Adv Funct Mater 2005;15(12):2016–20.

[4] Shen Y, Lin YH, Li M, Nan CW. High dielectric performance of polymer interparticle barrier layer. Adv Mater 2007;19(10):1418–22.

[5] Ma C, Zhang W, Zhu YF, Ji LJ, Zhang RP, Koratkar N, et al. In-situ alignment and dispersion of functionalized carbon nanotubes in polymer composites by AC electric field. Carbon 2008;46(4):706–10.

[6] Zhang Q, Huang J-Q, Qian W-Z, Zhang Y-Y, Wie F. The road for nanomaterials industry: a review of carbon nanotube production, post-treatment, and bulk applications for composites and energy storage. Small 2013;9(8):1237–65.

[7] Demczyk BG, Wang YM, Cumings J, Hetman M, Han W, Zettl A, et al. Direct mechanical measurement of the tensile strength and elastic modulus of multiwalled carbon nanotubes. Mater Sci Eng-A 2002;334(1–2):173–8.

[8] Tans SJ, Devoret MH, Groeneveld RJA, Dekker C. Electron-electron correlations in carbon nanotubes. Nature 1998;394(6695):761–4.

[9] Hamada N, Sawada S, Oshiyama A. New one-dimensional conductors: graphitic microtubules. Phys Rev Lett 1992;68(10):1579–81.

[10] Pötschke P, Bhattacharyya AR, Janke A. Carbon nanotube-filled polycarbonate composites produced by melt mixing and their use in blends with polyethylene. Carbon 2004;42(5–6):965–9.

[11] Villmow T, Pötschke P, Pegel S, Häussler L, Kretzschmar B. Influence of twin-screw extrusion conditions on the dispersion of multi-walled carbon nanotubes in a poly(lactic acid) matrix. Polymer 2008;49(16):3500–9.

[12] Pegel S, Pötschke P, Petzold G, Alig I, Dudkin SM, Lellinger D. Dispersion, agglomeration, and network formation of multiwalled carbon nanotubes in polycarbonate melts. Polymer 2008;49(4):974–84.

[13] Müller MT, Krause B, Pötschke P. A successful approach to disperse MWCNTs in polyethylene by melt mixing using polyethylene glycol as additive. Polymer 2012;53(15):3079–83.

[14] Arjmand M, Mahmoodi M, Gelves GA, Park S, Sundararaj U-T. Electrical and electromagnetic interference shielding properties of flow-induced oriented carbon nanotubes in polycarbonate. Carbon 2011;49(11):3430–40.

[15] Kim HM, Kim K, Lee CY, Joo J, Cho SJ, Yoon HS, et al. Electrical conductivity and electromagnetic interference shielding of multiwalled carbon nanotube composites containing Fe catalyst. Appl Phys Lett 2004;84(4):589–91.

[16] Yang YL, Gupta MC, Dudley KL, Lawrence RW. Novel carbon nanotube-polystyrene foam composites for electromagnetic interference shielding. Nano Lett 2005;5(11):2131–4.

[17] Arjmand M, Apperley T, Okoniewski M, Sundararaj U-T. Comparative study of electromagnetic interference shielding properties of injection molded versus compression molded multi-walled carbon nanotube/polystyrene composites. Carbon 2012;50(14):5126–34.

[18] Li N, Huang Y, Du F, He XB, Lin X, Gao HJ, et al. Electromagnetic interference (EMI) shielding of single-walled carbon nanotube epoxy composites. Nano Lett 2006;6(6):1141–5.

[19] Liu ZF, Bai G, Huang Y, Ma YF, Du F, Li FF, et al. Reflection and absorption contributions to the electromagnetic interference shielding of single-walled carbon nanotube/polyurethane composites. Carbon 2007;45(4):821–7.

[20] Yang C, Lin Y, Nan C-W. Modified carbon nanotube composites with high dielectric constant, low dielectric loss and large energy density. Carbon 2009;47(4):1096–101.

[21] Liu H, Shen Y, Song Y, Nan C-W, Lin Y, Yang X. Carbon nanotube array/polymer core/shell structured composites with high dielectric permittivity, low dielectric loss, and large energy density. Adv Mater 2011;23(43):5104–8.

[22] Martinelli NG, Savini M, Muccioli L, Olivier Y, Castet F, Zannoni C, et al. An atomistic description of polymer dielectrics/pentacene interfaces: influence of electrostatic interactions on charge mobility values. Adv Funct Mater 2009;19(20):3254–61.

[23] Gao J, Asadi K, Xu JB, An J. Controlling of the surface energy of the gate dielectric in organic field-effect transistors by polymer blend. Appl Phys Lett 2009;94:093302–93303.

[24] Dimiev A, Lu W, Zeller K, Crowgey B, Kempel LC, Tour JM. Low-loss, high-permittivity composites made from graphene nanoribbons. ACS Appl Mater Interfaces 2011;3(12):4657–61.

[25] Calame JP. Finite difference simulations of permittivity and electric field statistics in ceramic-polymer composites for capacitor applications. J Appl Phys 2006;99:084101–84111.

[26] Stefanescu EA, Tan XL, Lin ZQ, Bowler N, Kessler MR. Multifunctional PMMA-ceramic composites as structural dielectrics. Polymer 2010;51(24):5823–32.

[27] Alkoy EM, Dagdeviren C, Papila M. Processing conditions and aging effect on the morphology of PZT electrospun nanofibers, and dielectric properties of the resulting 3–3 PZT/Polymer composite. J Am Ceram Soc 2009;92(11):2566–70.

[28] Okamoto M, Nam PH, Maiti M, Kotaka T, Nakayama T, Takada M, et al. Biaxial flow-Induced alignment of silicate layers in polypropylene/clay nanocomposite foam. Nano Lett 2001;1(9):503–5.

[29] Motlagh GH, Hrymak AN, Thompson MR. Improved through-plane electrical conductivity in a carbon-filled thermoplastic via foaming. Polym Eng Sci 2008;48(4):687–96.

[30] Ameli A, Jung PU, Park CB. Through-plane electrical conductivity of injection-molded polypropylene/carbon-fiber composite foams. Comp Sci Tech 2013;76:37–44.

[31] Ameli A, Jung PU, Park CB. Electrical properties and electromagnetic interference shielding effectiveness of polypropylene/carbon fiber composite foams. Carbon 2013;60:379–91.

[32] McLachlan DS, Chiteme C, Heiss WD, Wu J. Fitting the DC conductivity and first order AC conductivity results for continuum percolation media, using percolation theory and a single phenomenological equation. Phys B: Condens Matter 2003;338(1–4):261–5.

[33] Xu X-B, Li Z-M, Shi L, Bian X-C, Xiang Z-D. ultralight conductive carbon-nanotube-polymer composite. Small 2007;3(3):408–11.

[34] Harikrishnan G, Singh SN, Kiesel E, Macosko CW. Nanodispersions of carbon nanofiber for polyurethane foaming. Polymer 2010;51(15):3349–53.

[35] Tran M-P, Detrembleur C, Alexandre M, Jerome C, Thomassin J-M. The influence of foam morphology of multi-walled carbon nanotubes/poly(methyl methacrylate) nanocomposites on electrical conductivity. Polymer 2013;54(13):3261–70.

[36] Thomassin J-M, Pagnoulle C, Bednarz L, Huynen I, Jerome R, Detrembleur C. Foams of polycaprolactone/MWNT nanocomposites for efficient EMI reduction. J. Mater Chem 2008;18:792–6.
[37] Thomassin J-M, Huynen I, Jeromea R, Detrembleur C. Functionalized polypropylenes as efficient dispersing agents for carbon nanotubes in a polypropylene matrix; application to electromagnetic interference (EMI) absorber materials. Polymer 2010;51(1):115–21.
[38] Thomassin J-M, Vuluga D, Alexandre M, Jerome C, Molenberg I, Huynen I, et al. A convenient route for the dispersion of carbon nanotubes in polymers: application to the preparation of electromagnetic interference (EMI) absorbers. Polymer 2012;53(1):169–74.
[39] Hermant MC, Verhulst M, Kyrylyuk AV, Klumperman B, Koning CE. The incorporation of single-walled carbon nanotubes into polymerized high internal phase emulsions to create conductive foams with a low percolation threshold. Comp Sci Tech 2009;69(5):656–62.
[40] Zhang HB, Yan Q, Zheng WG, He Z, Yu ZZ. Tough graphene–polymer microcellular foams for electromagnetic interference shielding. ACS Appl Mater Interfaces 2011;3(3):918–24.
[41] Antunes M, Mudarra M, Velasco JI. Broadband electrical conductivity of carbon nanofibre-reinforced polypropylene foams. Carbon 2011;49(2):708–17.
[42] McNally T, Pötschke P, Halley P, Murphy M, Martin D, Bell SEJ, et al. Polyethylene multiwalled carbon nanotube composites. Polymer 2005;46(19):8222–32.
[43] Meincke O, Kaempfer D, Weickmann H, Friedrich C, Vathauer M, Warth H. Mechanical properties and electrical conductivity of carbon-nanotube filled polyamide-6 and its blends with acrylonitrile/butadiene/styrene. Polymer 2004;45(3):739–48.
[44] Du F, Fischer JE, Winey KI. Effect of nanotube alignment on percolation conductivity in carbon nanotube/polymer composites. Phys Rev B 2005;72:121404(R).
[45] Munson-McGee SH. Estimation of the critical concentration in an anisotropic percolation network. Phys Rev B 1991;43(4):3331–6.
[46] Choi ES, Brooks JS, Eaton DL, Al-Haik MS, Hussaini MY, Garmestani H, et al. Enhancement of thermal and electrical properties of carbon nanotube polymer composites by magnetic field processing. J Appl Phys 2003;94(9):6034–9.
[47] Adler J, Meir Y, Aharony A, Harris AB, Klein L. J Stat Phys 1990;58(3–4):511–38.
[48] Gingold DB, Lobb CJ. Percolative conduction in three dimensions. Phys Rev B 1990;42(13):8220–4.
[49] Pötschke P, Dudkin SM, Alig I. Dielectric spectroscopy on melt processed polycarbonate-multiwalled carbon nanotube composites. Polymer 2003;44(17):5023–30.
[50] Karasek L, Meissner B, Asai S, Sumita M. Percolation concept: polymer-filler gel formation, electrical conductivity and dynamic electrical properties of carbon-black-filled rubbers. Polym J 1996;28(2):121–6.
[51] Kolb M, Botet R, Jullien R. Scaling of kinetically growing clusters. Phys Rev Lett 1983;51(13):1123–6.
[52] Stankovich S, Dikin DA, Dommett GHB, Kohlhaas KM, Zimney EJ, Stach EA, et al. Graphene-based composite materials. Nature 2006;442:282–6.
[53] Panwar V, Park J-O, Park S-H, Kumar S, Mehra RM. Electrical, dielectric, and electromagnetic shielding properties of polypropylene-graphite composites. J Appl Polym Sci 2010;115(3):1306–14.
[54] Yuan JK, Yao SH, Dang ZM, Sylvestre A, Genestoux M, Bai J. Giant dielectric permittivity nanocomposites: realizing true potential of pristine carbon nanotubes in polyvinylidene fluoride matrix through an enhanced interfacial interaction. J Phys Chem 2011;115(13):5515–21.
[55] Jiang M-J, Dang Z-M, Bozlar M, Miomandre F, Bai J. Broad-frequency dielectric behaviors in multiwalled carbon nanotube/rubber nanocomposites. Appl Phys 2009;106(8):084902–84906.
[56] Mahmoodi M, Arjmand M, Sundararaj U-T, Park S. The electrical conductivity and electromagnetic interference shielding of injection molded multi-walled carbon nanotube/polystyrene composites. Carbon 2012;50(4):1455–64.
[57] Watts PCP, Hsu WK, Randall DP, Kroto HW, Walton DRM. Non-linear current–voltage characteristics of electrically conducting carbon nanotube–polystyrene composites. Phys Chem Chem Phys 2002;4(22):5655–62.
[58] Effros AL, Shklovskii BI. Critical behaviour of conductivity and dielectric constant near the metal-non-metal transition threshold. Phys Status Solidi B 1976;76(2):475–85.
[59] Tamura R, Lim E, Manaka T, Iwamotoa MJ. Analysis of pentacene field effect transistor as a Maxwell–Wagner effect element. Appl Phys 2006;100(11):114515–7.